Ultrasensitive Electrochemical Sensors based on Cu and Cu@Ag Nanorods for Simultaneous Heavy Metal Detection

Smruti Ranjan Dash[a,b], Subhendu Sekhar Bag[b,c], Animes Kumar Golder[b,d,*] and Aruna Ivaturi[a*]

[a]Smart Materials Research and Device Technology (SMaRDT) Group, WestCHEM, Department of Pure and Applied Chemistry, University of Strathclyde, Glasgow G1 1XL, UK

[b]Centre for the Environment, Indian Institute of Technology Guwahati, Assam-781039, India

[c]Department of Chemistry, Indian Institute of Technology Guwahati, Assam-781039, India

[d]Department of Chemical Engineering, Indian Institute of Technology Guwahati, Assam-781039, India

*Corresponding authors

Email:

aruna.ivaturi@strath.ac.uk; Tel: +44-141-5484398; Fax: +44-141-5484822

animes@iitg.ac.in; Tel: +91-361-2582269; Fax: +91-361-2582292

Abstract

This work reports the development of ultrasensitive miniaturized electrochemical device for heavy metal sensing. A laser engraver based patterning of fluorine-doped tin oxide (FTO) sheet was done to draw an etched pattern forming a miniaturized 3-electrode configuration. A layer of Ag/AgCl ink served as pseudo-reference electrode. The sensing electrode was coated using low-cost Cu nanorods (CuNRs) grown radially along the {110} surface with aspect ratio of 8.0 and Cu@Ag core-shell nanorods (Cu@AgNRs) formed via galvanic displacement for simultaneous electrocatalytic detection of heavy metal ions (Pb(II), Cd(II), Hg(II), and Zn(II)) present in water. The electroactive surface area of the prepared devices is 0.026, 0.093 and 0.125 cm^2 for bare FTO, CuNRs/FTO and Cu@AgNRs/FTO, respectively. Bimetal Cu@AgNRs/FTO sensor exhibited the lowest limit of detection of 1, 2, 5 and 6 nM, respectively, detecting Cd(II), Pb(II), Zn(II), and Hg(II) ions, and it was 2, 2, 3 and 4 nM, respectively, for simultaneous detection of Zn(II), Pb(II), Cd(II) and Hg(II). The Cu@AgNRs/FTO based device showed distinct peak-to-peak separation by 0.40, 0.25 and 0.51 V for Zn(II)-Cd(II), Cd(II)-Pb(II) and Pb(II)-Hg(II), respectively. This device was highly sensitive (583.6-1261.8 $\mu A.\mu M^{-1}.cm^{-2}$) for heavy metal detection over CuNRs/FTO (15.9-107.4 $\mu A.\mu M^{-1}.cm^{-2}$). The Cu@AgNRs/FTO based sensors demonstrated good reproducibility (relative standard deviation ≤ 5%) with recovery (> 90%) in the case of all target heavy metals simultaneously present in environmental water samples. Hence, the Cu nanorods based miniaturized sensing platforms developed in the present study for simultaneous heavy metal detection are potential low-cost alternatives providing a repeatability of upto 4 cycles unlike the commercial screen-printed electrodes.

Keywords: FTO substrates; Electrochemical sensing platform; Toxic heavy metals; Square wave anode stripping voltammetry

1. Introduction

Environmental monitoring is one of the most critical issues that is given the highest priority by the authorities. The regulating bodies are making waste disposal parameters stricter and stricter over the period. On the other hand, rapid industrialization and extensive agricultural practices have seen an increased use of pesticides and insecticides that lead to heavy metals (HMs) contamination in water and soil.[1,2] These HMs end up entering into the food chain, thereby destabilizing the ecosystem. Intake of HMs more than the allowable limits could affect humans in various ways leading to reproductive disorders [3], respiratory diseases[4], and neural disorders [5]. On entering the human body, Pb(II) ions affect the nervous system and hinder their reasoning and intelligence capability.[6] Similarly, Cd(II) ions are known to bioaccumulate in the human body and could affect the bones, kidney and liver. Hg(II) ions persist in nature and affect human by degenerating the kidneys and causes various cardiovascular issues.[7] The source of Zn(II) in the environment is the uncontrolled disposal of industrial wastes such as metal plating industries into land and water bodies. Though a small amount of zinc is necessary as a macronutrient in human bodies, an excessive intake of Zn(II) has shown to affect the bone mass density and cause renal problems.[8]

Many detection techniques such as atomic absorption spectroscopy,[9] inductively coupled plasma mass spectroscopy,[10] inductively coupled plasma emission spectroscopy[11] and colorimetric methods[12] have been developed for the ultrasensitive detection of these heavy metal ions. However, these methods beset with high installation costs and limitations for on-field applications. Electrochemical techniques on the other hand are low-cost, highly sensitive and selective towards the target analyte(s). The miniaturized systems like screen-printed electrodes have been proven to be useful for on-field applications.[13–15] Further, modification of the

working electrodes with nanomaterials has shown improved electrokinetic and electrocatalytic activities along with improved electrical conductivity.[16–19] For instance, the Au@Ag core-shell nanoparticles have been used in fabricating electrochemical sensors with enhanced Hg(II) sensing.[20] In our previous report, we have also reported that bi-metallic Ag@Pt core-shell nanoparticles could notably enhance sensitivity towards the detection of Pb(II) ions in the presence of other HMs ions.[21] Moreover, modification of the nanoparticles' surface could further enhance the electrocatalytic response towards HMs sensing. Modifying the electrode surface with metal nanoparticles[22–25], conductive polymers[26–29], ionic-liquids [30,31], etc. to increase the sensitivity of electrochemical sensors along with the use of specialized electrodes like boron doped diamond electrodes[32], gold electrodes[33], etc have been reported. Copper nanoparticles have been extensively used for the electrochemical sensing of drugs [34] , conductive inks [35] and pesticides [36,37].

The use of copper nanoparticles/reduced graphene oxide (RGO) composites have previously been reported for the electrochemical sensing of HMs ions like Cd(II), Pb(II) and Hg(II).[38] However, copper nanoparticles are often demerited by quick oxidation thereby altering the surface properties and interaction with the analytes.[39] Thus, it is most often coated by a noble metal nanocatalyst to prevent oxidation[40] and to provide nanoporous channels which is known to enhance the electrochemical sensitivity of the catalyst by providing a confined area for the electrochemical reactions to take place.[41,42] Metal nanoparticles like Au[43] and Ag[21] and metal oxide nanoparticles like SnO_2[44], NiO[45] and Fe_3O_4[46] have been used in previous instances for HMs detection. In this work, we have introduced Fluorine doped tin oxide (FTO) based miniaturized three-electrode sensing devices based on Cu nanorods

(CuNRs) and Cu@Ag core-shell nanorods (Cu@AgNRs) as sensing modifiers. FTO exhibits high electrical conductivity, ensuring efficient charge transfer during electrochemical processes [47]. Moreover, FTO demonstrates excellent chemical stability and corrosion resistance under diverse environmental conditions, ensuring long-term durability in electrochemical devices. Furthermore, FTO electrodes are compatible with various surface modifications, allowing for tailored surface properties to enhance specific functionalities, such as catalytic activity or surface modifications [48]. These combined properties make FTO a versatile and reliable choice for electrochemical sensors, facilitating sensitive and selective detection of heavy metal ions. The sensing devices (CuNRs/FTO and Cu@AgNRs/FTO) exhibit ultrasensitive electrocatalytic detection of Zn(II), Cd(II), Pb(II), and Hg(II) ions present together in various environmental water samples.

2. Materials and methods

2.1 Synthesis of CuNRs and Cu@AgNRs

Copper nanorods (CuNRs) were synthesized using a method previously described in literature, with slight modifications.[49] All chemicals used in this study were of analytical grade obtained from Sigma Aldrich/Merck, UK. Deionized water (18.2 MΩ) obtained from a Milli Q water purifier system (Millipore Ltd.) was used in all experiments. CuNRs were synthesized using $CuCl_2$ as the source of Cu, sodium chloride (NaCl) as an additive, polyvinylpyrollidone (PVP K40) as a capping agent, and L(+)-ascorbic acid (AA) as a reducing agent. $CuCl_2$ and AA precursor solutions were prepared separately by dissolving 0.1 M anhydrous $CuCl_2$ and 1.5 M AA (1.5 M) in deionized water under ultrasonication for 0.5 h. 2.4% (w/v) PVP K40 and 0.35 M NaCl

were added into the AA precursor solution under constant stirring. The resulting mix was then added to the $CuCl_2$ precursor solution. The bluish green colour of $CuCl_2$ solution immediately turned white as soon as the AA, PVP and NaCl were added into it. This could be due to the formation of $CuCl^-$ precipitate due to reduction in the presence of high concentration of AA. pH of the final precursor solution was adjusted to 3.5 by adding 4 M NaOH (~2 mL), and the final reaction volume was adjusted to 60 mL. The precursor mix was then equally divided into two into autoclavable bottles at the reaction temperature was maintained at 80 °C using a thermostatic and thermo stirring hot water bath (Make: Clifton, Model: NE4-HT, North Sommerset, UK) for 24 h. The image of the progression of CuNRs formation is provided in Figure S1 of the Supplementary Information. The as-synthesized copper nanorods (CuNRs) were washed thrice using 1:1 (v/v) ethanol and water followed by centrifugation (3000 rpm for 15 min) and stored (1 $mg.mL^{-1}$) in a storage solution comprising of 1 M AA and 2.4% (w/v) PVP K40 in water. Before further using the as-synthesized CuNRs, the dispersion was thoroughly washed again with DI water thrice by repeating centrifugation (at 3000 rpm for 15 min) and re-dispersion in to remove the AA and PVP K40 from the CuNRs.[50] The final concentration was adjusted to 1 $mg.mL^{-1}$ using DI water. For the synthesis of Cu-Ag core-shell nanorods (Cu@AgNRs), a 10 mL portion of the CuNRs solution stored in the storage solution was taken and 0.5 mL of 0.025 M $AgNO_3$ solution was mixed into it and vigorously shaken to get a uniform mixture utilizing the AA and PVP in the storage solution for the reduction and stabilization process of Ag over CuNRs. and vigorously shaken to get a uniform mixture. It was then allowed to stand undisturbed for 2 h for the reaction to complete.[50] Similar washing

procedure as that of CuNRs was employed to obtain Cu@AgNRs solution in water for immediate use.

2.2 Fabrication of three-electrode miniature system based on FTO

A laser engraver (Make: Epilog Laser Engraver Model: Helix, Clavedon, UK) was used for patterning the FTO coated glass (Make: NSG Pilkington: Model: TEC 7, Lancashire, UK). The etching was performed based on the pattern shown in Figure 1a and parameters developed using AutoCAD software resulting in pattern shown in Figure 1b. The etching parameters were set at 85% laser power with a frequency of 5000 Hz. The scanning speed was maintained at 20% of the maximum capacity. A layer of Ag/AgCl ink (~0.5 mm thick) (ASL Co., Japan) was coated, by doctor blading method, on one of the sections of the FTO that acts as the reference electrode (Figure 1c). The other part of the electrode was masked using two layers of scotch tape which prevented the smudging of the Ag/AgCl ink onto other sections of the patterned FTO during doctor blading. In the next step the nanocatalysts (CuNRs or Cu@AgNRs, washed and suspended in DI water) were added by drop casting 60 μL of nanocatalyst solution onto an area of ~0.7 × 0.7 cm^2 and 100 μL of 0.5% Nafion solution in iso-propanol and dried at 60 °C in a hot air oven to fabricate the miniature three electrode system (Figures 1d and 1e). Slow drying of the nanomaterial ink in the presence of Nafion forms a viscous gel like substance. This stops particles from flowing to the edges of the droplet, enabling them to be deposited evenly. Thus, avoiding the coffee ring effect.

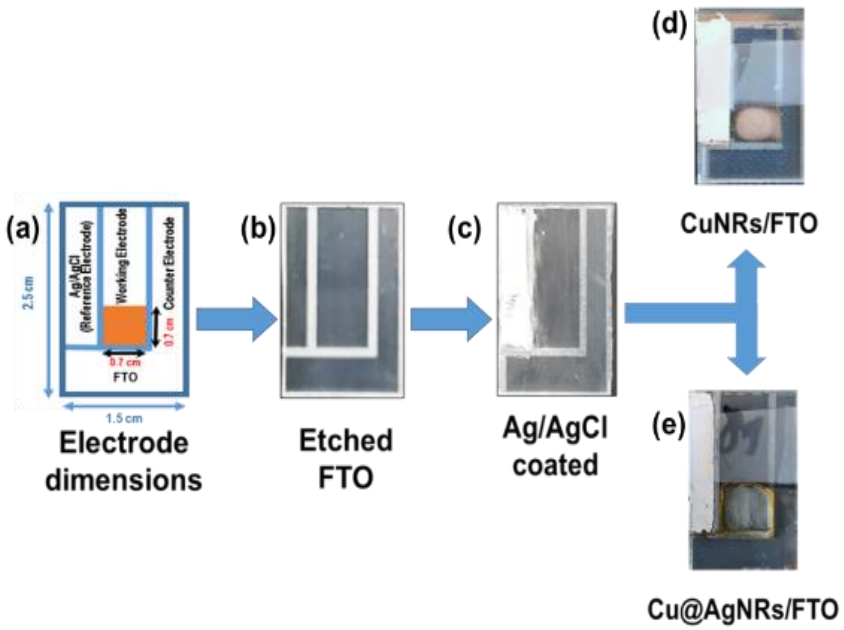

Figure 1: Step by step method to fabricate the compact three-electrode system for targeted sensing of heavy metals.

2.3 Material and device characterizations

Optical absorbance of the synthesized CuNRs and Cu@AgNRs was measured using UV–Vis spectrophotometer (Make: Shimadzu, Model: UV-3101, Buckinghamshire, UK). The crystallinity of the synthesized material was characterized using X-ray powder diffractometer (Make: Rigaku, Model: Micromax-007HF, CA, USA) equipped with Cu-Kα radiation source (α = 1.541 Å), scanned in the 2θ range from 30° to 90° with a step speed of 10° per min. Morphology of CuNRs and Cu@AgNRs were characterized by Field emission transmission electron microscopy (FETEM, Make: JEOL, Model: JEM-2100F, Tokyo, Japan). The surface functional groups were analyzed by using FT-IR spectrometer equipped with a MIR detector (Make: Perkin Elmer, Model: Spectrum two, Waltham, USA). Anions present in water samples were analyzed by using an Ion chromatography (Metrohm, 930 Compact IC Flex, using a 6.1006.530 Metrosep A Supp

5-250 column). The run time of 30 min was applied using an eluent containing a mixture of 1.0 mM $NaHCO_3$ and 3.3 mM Na_2CO_3 in DI water with a flow rate of 0.7 $mL.min^{-1}$.

All electrochemical measurements were performed at room temperature on the fabricated miniaturized three electrode system where CuNRs or Cu@AgNRs modified FTO served as the working electrode, bare FTO as an auxiliary electrode and Ag/AgCl ink as a reference electrode (Figures 1d and 1e), using potentiostat/ galvanostat (Make: Metrohm Model: PGSTAT 302N, Kanaalweg, The Netherlands). A pictorial view of the sensing system is provided in Figure S2 of the Supplementary Information.

Electrochemical impedance spectroscopy (EIS) was carried out using 1 mM potassium ferricyanide in 0.1 M KCl to determine the electrode resistance exhibited by the devices. Bare FTO was first measured using EIS to generate the corresponding Nyquist plot, which was then fitted using Nova 2.1.4 software from Metrohm.

Electrochemical sensing of Zn(II), Cd(II), Pb(II), and Hg(II) ions was performed using Square wave anodic stripping voltammetry (SWASV) in the potential range of −1.4 to 0.5 V vs. Ag/AgCl with an amplitude of 0.02 V and pulse width of 0.05 s. Either CuNRs or Cu@AgNRs modified FTO was subjected to 250 µL of 0.1 M acetate buffer solution at pH 5 and the target HMs ions at the desired concentrations for the SWASV analysis. These parameters were adopted from our previous work for electrochemical detection of Pb(II).[21] The analytes (here HMs) were then deposited (pre-concentrated) onto working electrode surface by reducing them at -0.4 V for 90 s and subsequently stripped off from the electrode surface into the electrolytic solution by varying the potential in the opposite direction (based on individual oxidation potentials) within the predetermined potential range. The deposition potential was chosen as -0.4 V. vs. AgCl as further increase in the potential during the optimization stage (data not shown)

delaminated the tin coating from the FTO glass severely affecting the workability of the electrode.

2.4 Real water sample analysis

The viability of the fabricated electrochemical sensors for HMs detection was investigated using environmental water samples collected from Clyde River, Glasgow (UK) and tap water from the University of Strathclyde Campus. The collected water samples were stored in a refrigerator at 4 °C to preserve the characteristics and were used without any pretreatment. The anions (chloride, fluoride, nitrate, sulphate and phosphate) concentrations in the collected samples were determined using ion chromatography. The effect of the presence of these anions on the simultaneous electrochemical sensing of HMs was determined by preparing the electrolyte using the collected water samples instead of the DI water and spiking the water samples with the required amount of HMs ions. The sensing performance was then evaluated by obtaining the square wave voltammograms with the optimized sensing parameters.

3. Results and discussions

3.1 Characterization of CuNRs and Cu@AgNRs

Figure 2 shows the UV-vis spectroscopic analysis of the synthesized CuNRs and Cu@AgNRs dispersed in water. A distinct broad peak is observed at λ=592 nm for CuNRs (black) which is indicative of the formation of copper nanorods.[51] It can be observed that on reaction with $AgNO_3$ for 2 h, the SPR peak due to copper is masked by the SPR peak of Ag (λ=431 nm, red). This is due to the deposition of Ag over the CuNRs. The deposition of Ag on CuNRs can be attributed to the galvanic displacement,

which is further augmented by the presence of AA. PVP in the reaction solution helps in stabilizing the prepared Cu@AgNRs. Similar results were obtained in our previous studies on the synthesis of Ag@Pt core-shell nanoparticles where the SPR peak of the core (Ag) was masked by the deposition of Pt (shell) over it.[21]

Figures 3a and 3b shows the XRD pattern of CuNRs and Cu@AgNRs, respectively. The three dominant peaks in Figure 3a at 2θ = 43.5°, 50.3° and 74.1° correspond, respectively, to the diffraction from (111), (200) and (220) planes of face-cantered cubic (FCC) Cu (PDF card #00-004-0836, Figure 3c). Similarly, in the case of Cu@AgNRs (Figure 3b), the diffraction from (111), (200), (220), (311) and (222) planes at 2θ angle 38.2°, 44.2°, 64.4°, 77.5° and 81.5° corresponds to FCC Ag (PDF card #01-077-6540, Figure 3c). Few unassigned peaks (much lower intensity than Cu and Ag peaks) at 2θ angle 35.8°, 42.1°, 46.6°, 51.1° and 51.8° could be due to the organic substances contributed by ascorbic acid, PVP and trace amount of NaCl (additive) that may be present on the nanorods as reducing and stabilizing agents.[52,53]

The FT-IR analysis of the synthesized CuNRs and Cu@AgNRs is presented in Figures S3a-S3b of the Supplementary Information. The results show similar features as the same reducing and stabilizing agents used in the formation of the CuNRs and Cu@AgNRs. The strong peak observed at 3450 cm^{-1} corresponds to the stretching vibration of the O-H adsorbed water group on the nanomaterial surface. C=O vibrations and out of ring C–H bonds, respectively, give rise to peaks at 1680 and 1384 cm^{-1} which could be due to the carboxylic acid functional group from the AA. The C-N vibration generates a small yet an important peak at around 1288 cm^{-1}, that proves the stabilization due to PVP. The only source of C-N bond is from the nitrogen present in the pyrrole ring in the PVP.

Figure 4a shows FETEM micrograph of typical CuNRs (average aspect ratio = 8.0). A close examination indicates that these NRs have a cyclic penta-twinned structure with five {111}-type twin boundaries arranged radially along the common {110} surface (Figure S4(a) of the Supplementary Information) which is a typical in the case of CuNRs. [54,55] Analysis of the diffraction pattern reveals, diffraction rings with lattice spacing of 0.225 nm and 0.144 nm corresponding to the (111) and (220) planes of FCC Cu, respectively (Figure S4(b) of the Supplementary Information).[56] Figure 4b shows the FETEM micrograph of the synthesized Cu@AgNRs. Irregular thin surface layer of Ag deposited over the CuNRs can be seen at a higher magnification (Figure 4c). HRTEM micrograph reveals the crystalline fringes with lattice spacing of 0.24 nm corresponding to (111) of FCC Ag (Figure 4d).[57,58] The elemental mapping (Figures 4e- 4g) and EDX analysis show the deposition of Ag over CuNRs, and the percentage composition of Ag was 21.3% (w/w) and Cu core was 78.8% (w/w).

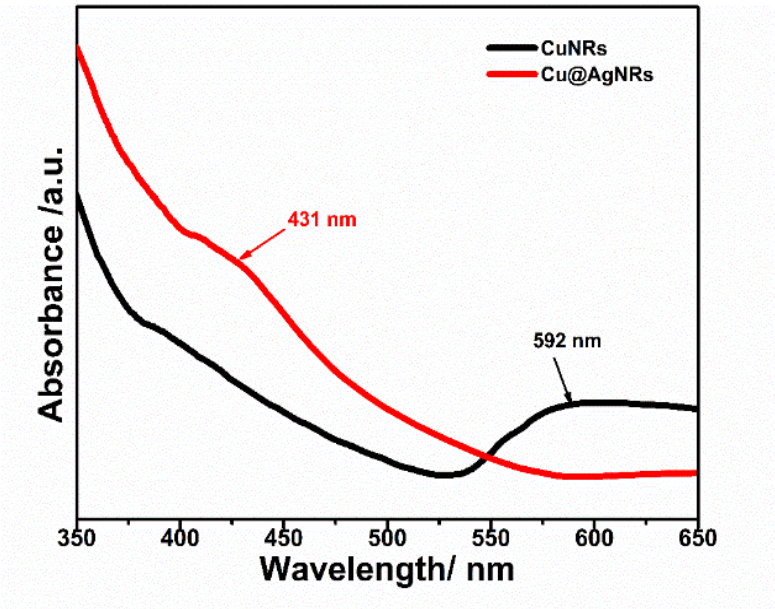

Figure 2: UV-vis spectroscopy analysis of the synthesized CuNRs and Cu@AgNRs.

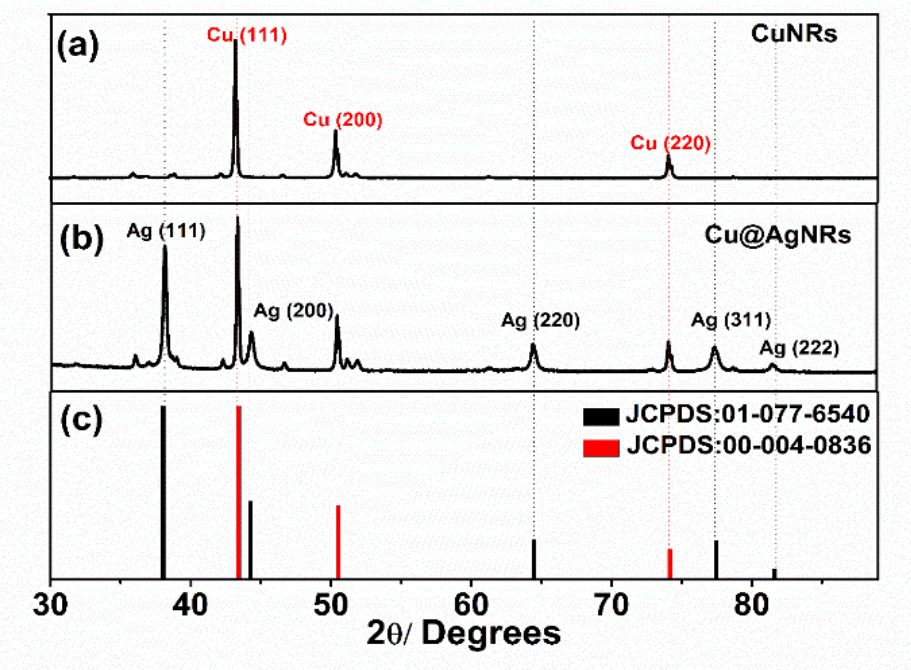

Figure 3: XRD analysis of the synthesized (a) CuNRs, (b) Cu@AgNRs, and (c) Corresponding JCPDS card.

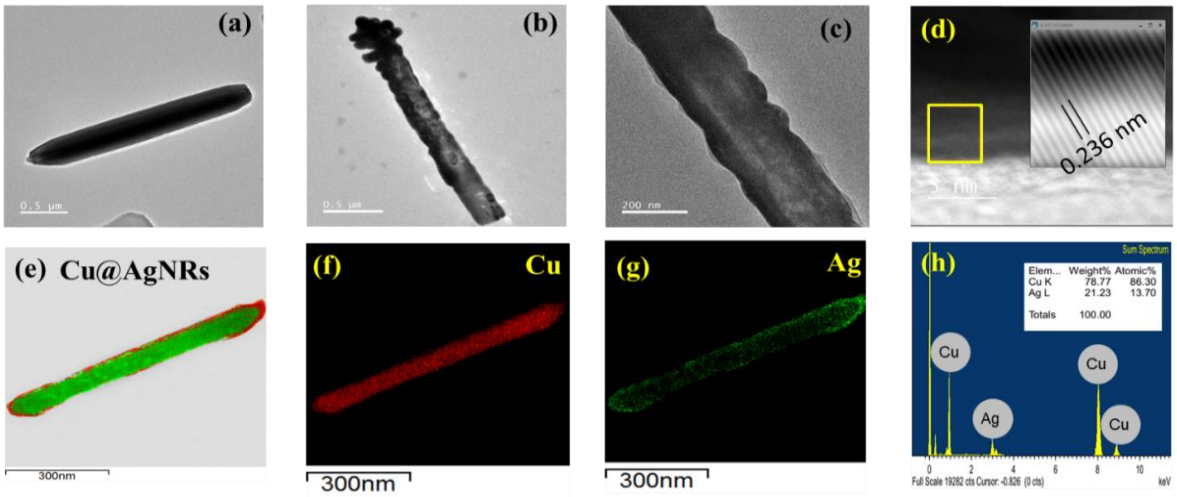

Figure 4: TEM micrographs of (a) CuNRs, (b and c) Cu@AgNRs, (d) HRTEM micrograph, (e) Elemental mapping, and Elemental distribution of (f) Copper, (g) Silver, and (h) EDX spectra and the elemental composition of Cu@AgNRs.

3.2 Electrochemical characterization of the fabricated electrodes

3.2.1 Electrochemical impedance spectroscopy (EIS)

Figure 5a gives the Nyquist plots showing the change in resistance as a function of surface modification of bare FTO (black curve), to CuNRs coated FTO (red curve) and Cu@AgNRs coated FTO (blue curve). The bare FTO electrode shows a resistance of 3.69 KΩ and a solution resistance of 96.5 Ω (Figure 5b). A Warburg component (which models the linear diffusion towards the electrode surface) was required to complete the circuit, which shows the heterogeneity and the diffusion limitation of the electrochemical system.[59,60] The Y_0 values of the Warburg component provides insights into how quickly analytes can diffuse to or from the electrode surfaces and it increases with the addition of different layers of electrocatalysts on the FTO as depicted in Figures 5a-5c.[61] Thus, a quiet time or a conditioning time of 30 s is provided before every experiment to reduce the effect of this diffusion limitation. The CuNRs/FTO and Cu@AgNRs/FTO shows the resistance of 2.91 and 2.35 kΩ, respectively, which is due to the increased conductivity induced by the presence of metal nanocomposites on its surface.

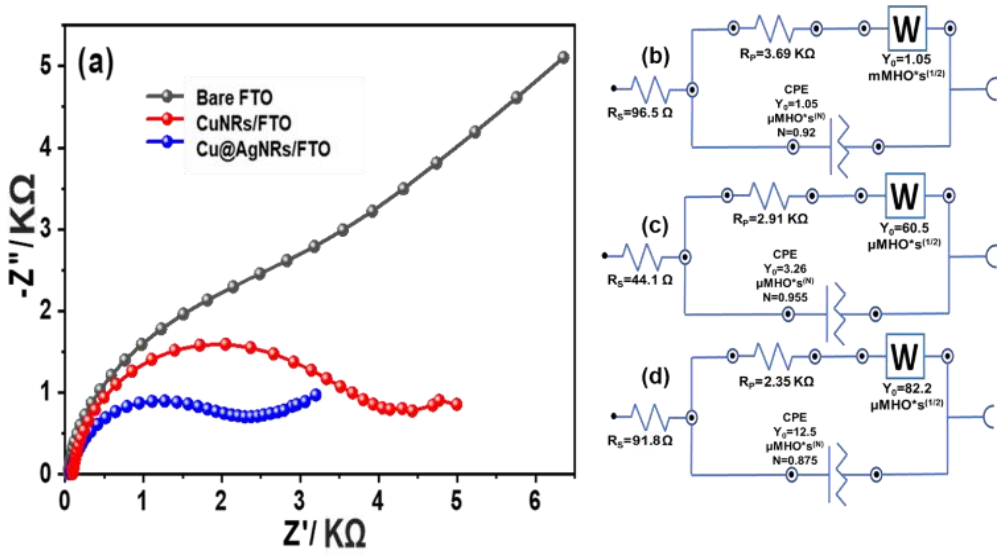

Figure 5: (a) Nyquist plot showing the change in resistances due to surface modifications of bare FTO (black curve), with CuNRs (red curve) or Cu@AgNRs (blue curve). (b)-(d) Corresponding equivalent circuits.

3.2.2 Estimation of electrochemical surface area

The electrochemical surface area was determined by using Randles -Sevcik relation (Eq. 1).[62,63]

$$I_P = 2.69 \times 10^5 A_{eff}\, D^{1/2} n^{3/2} \upsilon^{1/2}\, C_o \qquad (1)$$

Where n, υ, D and Co are the number of electrons involved in the electrochemical reaction, scan rate in $V \cdot s^{-1}$, diffusion coefficient in $cm \cdot s^{-1}$, and bulk concentration in $mol \cdot L^{-1}$ of the redox probe $K_3(Fe[CN_6])$, respectively. The cyclic voltammograms of each electrode at varying scan rates are presented in Figures 6a-6c. It can be seen that the peak currents gradually increased with the increase in the scan rate (5-200 $mV.s^{-1}$). The peak currents obtained in the case of Cu@AgNRs/FTO is the maximum followed by CuNRs/FTO. The increase in the peak current response was about 4 times in the case of CuNRs/FTO and 5 times in the case of ACu@AgNRs/FTO. In the case of modified electrodes, the shift of the peak positions to lower potentials is indicative of an enhanced electrokinetics activity. From the plot of I_{Pa} vs. $\upsilon^{0.5}$ (Figure 6d) and equating the slope values by considering D for $K_3(Fe[CN_6])$ of 6.67×10^{-6} cm^2 s^{-1} (n = 1) [64], A_{eff} was found to be 0.026, 0.093, and 0.125 cm^2, respectively for bare FTO, CuNRs/FTO and Cu@AgNRs/FTO. Their corresponding slope values were 0.0473, 1.671, and 2.24 ($\times 10^{-4}.A.V^{-0.5}.s^{0.5}$).

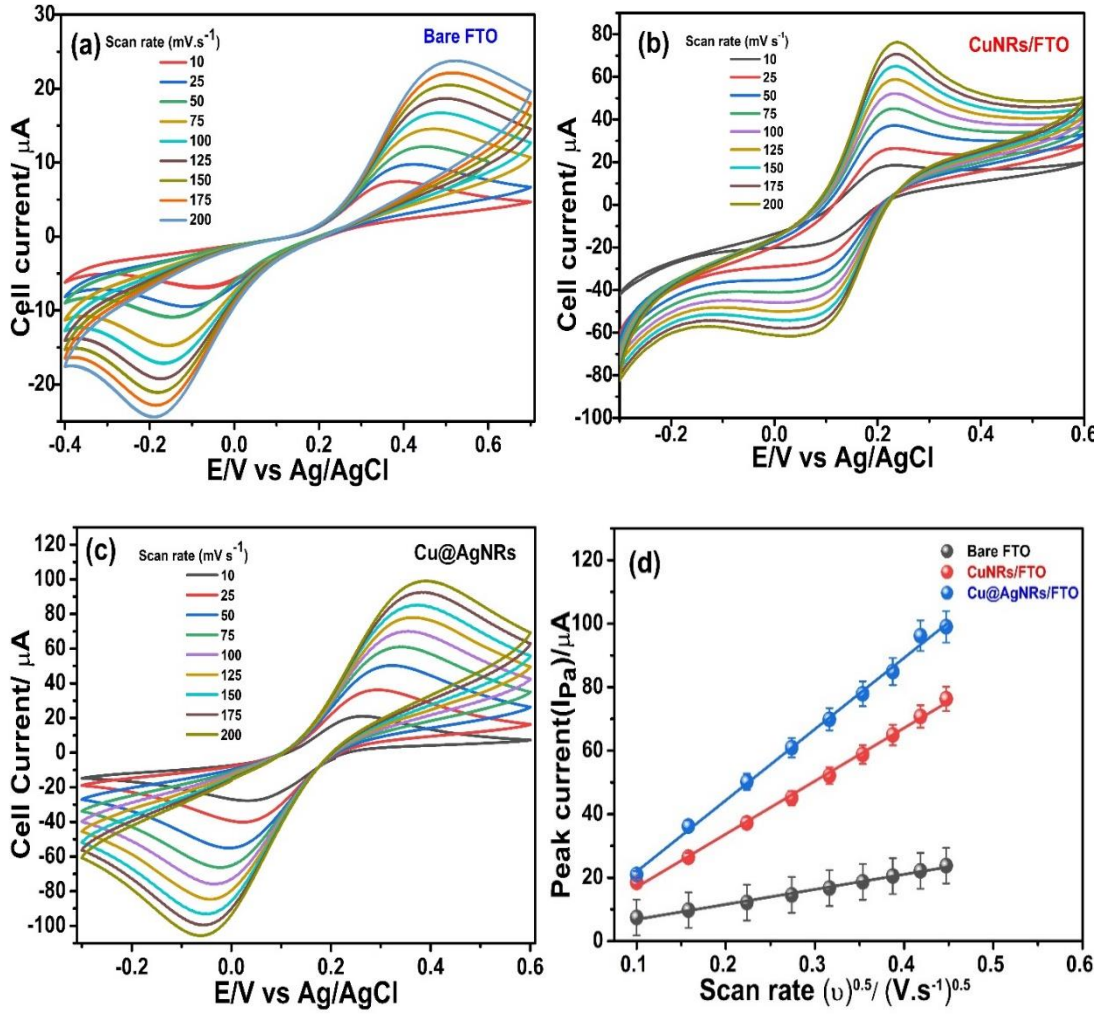

Figure 6: Cyclic voltammograms with different electrodes: (a) Bare FTO, (b) CuNRs/FTO and (c) Cu@AgNRs/FTO at various scan rates (10-200 mV.s−1) and (d) Variation of peak current (I_{Pa}) with square root of scan rate. Reaction conditions: $K_3(Fe[CN]_6)$ (1 mM) in 100 mL of 0.1 M KCl at ambient temperature.

3.2.3 Electrochemical sensing of HMs using CuNRs/FTO

The square-wave voltammetry method was used for HMs sensing using CuNRs/FTO. Figures 7a-7d show the current response for Zn(II), Cd(II), Pb(II), and Hg(II) ions, respectively. It can be seen that the peak potential obtained for Zn(II), Cd(II), Pb(II), and Hg(II) were, respectively at -1.3, -0.95, -0.50 and 0.15 vs. Ag/AgCl. Figure 7e

shows the calibration curves at various concentrations of HMs. The limit of detection (LoD), the limit of quantification (LoQ), and the sensitivity were calculated using the following relations (Eqs.2-4).[65]

$$LoD = 3S_b/m \quad (2)$$

$$LoQ = 10S_b/m \quad (3)$$

$$Sensitivity = m/A_{eff} \quad (4)$$

Where, S_b is the standard deviation of the blank electrolyte (number of experiments= 10), m is the slope of the calibration curve ($\mu A.\mu M^{-1}$) containing the lowest HMs concentration (0.1 µM) and A_{eff} is the effective surface area (cm^2) of the working electrodes. S_b was determined to be 0.125. The slope of the calibration curve was obtained from the corresponding linear equation (Eq. 1). LoD and LoQ for Zn(II) were calculated to be 0.005 and 0.017 µM. Similarly, for Pb(II), the LoD and LoQ were 0.007 and 0.026 µM. For Cd(II), it was, respectively 0.030 and 0.099 µM. However, the least response was obtained in the case of Hg(II), and the LoD and LoQ obtained, in this case, were 0.124 and 0.414 µM, respectively. This could be due to the formation of Hg-Cu amalgam that hinders the stripping response of the sensor. Similarly, at higher concentrations of Zn(II) (Figure 7a) and Cd(II) (Figure 7b), a shift in peak with additional shoulder peaks could be observed. This could be attributed to the formation of intermetallic compounds with CuNRs which interferes in the proper stripping of Zn [66] and Cd [67] from the surface, and the increased deposition layer (at higher concentrations) on the electrode surface hinders the mass transfer kinetics leading to shoulder peaks and peak shift.[68]

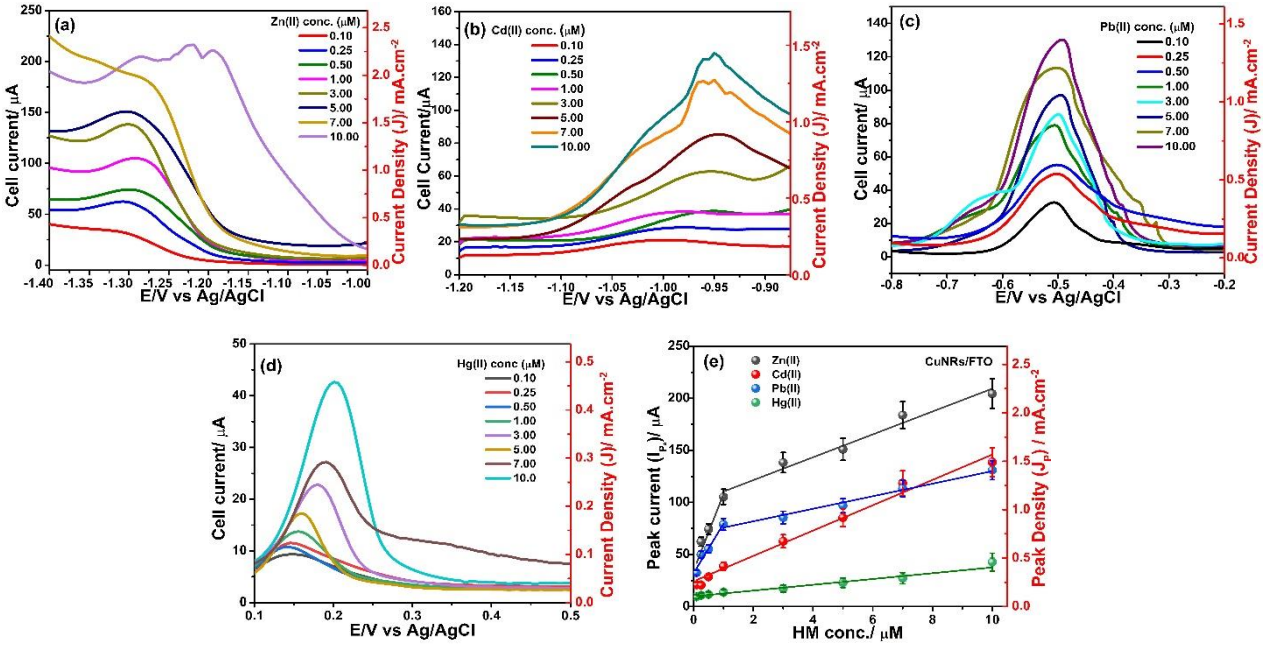

Figure 7: Square wave voltammograms recorded with different HMs ions: (a) Zn(II), (b) Cd(II), (c) Pb(II), (d) Hg(II), and (e) Corresponding calibration curves using CuNRs/FTO based miniature device. Reaction conditions: HMs 0.1-10 µM in acetate buffer at pH 5. Frequency was set at 15 Hz and amplitude 0.02 V, deposition time 90 s and conditioning time 30 s.

3.2.4 Electrochemical sensing of HMs using Cu@AgNRs/FTO

The electronic effect plays an important role in explaining charge transfer efficiencies in bi-metallic nanocatalysts. From monometallic to bi-metallic nanoparticles, an additional degree of freedom is introduced that enhances their electrocatalytic characteristics. Figure 8 shows the determination of Zn(II), Pb(II), Cd(II) and Hg(II) individually in 0.1 M of acetate buffer at pH 5 against the deposition potential of -0.4 V for 90 s at Cu@AgNRs/FTO. For Zn(II), Pb(II), Cd(II), and Hg(II) ions, the peak potential was noted at -1.3, -0.78, -0.55, and -0.4 V vs. Ag/AgCl, respectively (Figures 8a-8d). As the concentration of metal ions increased, the stripping current increased.

The corresponding calibration plot of various metal ions is depicted in Figure 8e. Two linear ranges could be observed which can be attributed to the change in the electrochemical reaction from diffusion-controlled domain at lower concentration to surface controlled reaction at higher concentration. Moreover, at higher concentration more HMs gets deposited on the working electrode surface and it becomes difficult for the system to strip all the HMs ions from the surface during the stripping phase of the SWASV process. Hence, it shows a dip in the calibration slope at higher concentrations thereby decreasing the sensitivity of the sensor. The sensing parameters for different HMs ions are summarized in Table 1. The sensitivity of Pb(II) was estimated to be approx. 1.1, 2.8, and 5.1 times higher as compared to Cd(II), Hg(II), and Zn(II). Again from Table 1, it can be observed that Cu@AgNRs/FTO showed an improved sensing of all HMs under consideration except for Zn(II) which showed a marginal increase in LoD value from 0.004 to 0.005 μM. This could be due to the bi-metallic interactions between Ag and Zn that might have reduced the electrocatalytic activity of the sensor towards Zn(II) [69].

The generation of shoulder peaks during SWASV for Hg(II) sensing (Figure 8d) could be attributed to the formation of mercury amalgam species on the electrode surface during the deposition step, leading to additional peaks associated with amalgam formation with Ag. [70] Additionally, interactions between mercury ions and other electroactive species present in the solution, such as competing metal ions can contribute to the appearance of shoulder peaks at higher concentrations.[66]

Table 1: Fabricated sensor performance parameters for individual HMs detection.

	Sensor parameters	**Zn(II)**	**Cd(II)**	**Pb(II)**	**Hg(II)**
	Permissible limits (USEPA, 2018) (µM)	76.5	0.044	0.072	0.01
CuNRs/FTO	Linear range (µM)	0.01-1 and 1-10			
	Linear equation (0.01-1 µM)	IPa(µA)= 88.39[Zn(II)] µM + 23.73	IPa(µA)= 19.84[Cd(II)] µM + 18.45	IPa(µA)= 58.90[Pb(II)] µM + 23.76	IPa(µA)= 3.11[Hg(II)] µM + 8.59
	R-squared	0.9	0.94	0.9	0.96
	LoD/LoQ (µM)	0.004/0.014	0.019/0.062	0.006/0.021	0.124/0.414
	Effective surface area (cm^2)	0.093			
	Sensitivity ($\mu A \cdot \mu M^{-1} \cdot cm^{-2}$)	116.76	26.2	77.8	4.1
Cu@AgNRs/FTO	Linear range (µM)	0.01-1.0 and 1.0-10	0.01-0.5 and 0.5-10	0.01-1.0 and 1.0-10	0.01-1 and 1-10
	Linear equation (0.01-1 µM)	I_{Pa}(µA)= 69.33[Zn(II)] µM + 40.67	I_{Pa}(µA)= 262.17[Cd(II)] µM + 20.68	I_{Pa}(µA)= 207.28[Pb(II)] µM + 22.62	I_{Pa}(µA)= 57.04[Hg(II)] µM + 20.55
	R-squared	0.9	0.94	0.98	0.94
	LoD/LoQ (µM)	0.005/0.017	0.001/0.004	0.002/0.006	0.006/0.021
	Effective surface area (cm^2)	0.125			
	Sensitivity ($\mu A \cdot \mu M^{-1} \cdot cm^{-2}$)	84.65	320.1	253.08	69.64

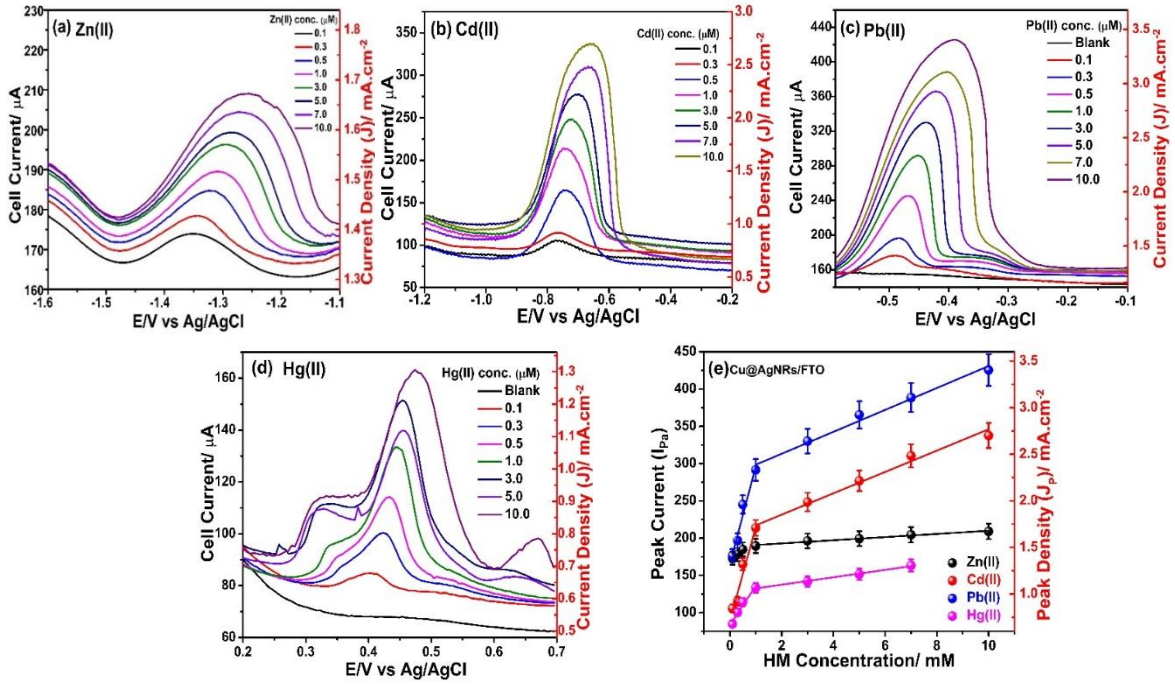

Figure 8: Square wave voltammograms measured with different HMs ions: (a) Zn(II), (b) Cd(II), (c) Pb(II), and (d) Hg(II) using Cu@AgNR/FTO based miniature device. Reaction conditions HMs 0.1-10 μM in acetate buffer at pH 5. Frequency was set at 15 Hz, amplitude 0.02 V, deposition time 90 s and conditioning time 30 s.

3.2.5 Simultaneous electrochemical sensing of HMs

Simultaneous detection and determination of Zn(II), Cd(II), Pb(II) and Hg(II) at bare FTO, CuNRs/FTO and Cu@AgNR/FTO was carried out in this study, and the SWASV signals were recorded simultaneously (Figure 9). It can be seen that blank FTO (Figure 9, black curve) could not produce any stripping signals for HMs, whereas CuNRs/FTO though could sense Cd(II), Pb(II) and Hg(II), but it was unable to give any signals for Zn(II) even at high concentration (1 μM). For Cu@AgNRs/FTO, well separated peaks were obtained. With the increase of each HMs concentration from 0.1 μM to 10 μM at a potential range of -1.4 V to +0.5 V vs Ag/AgCl, the maximum currents gradually increased.

Figures 10a and 10b show the SWASV signals for both the devices. For CuNRs/FTO, the best detection for Pb(II) was possible with an extended linear range from 0.25 to 10 µM. However, the detection of other HMs was poor. The detection of Zn(II) was possible only above the concentration of 1 µM, and the detection was ceased above the concentrations of 5 µM. Similarly, the detection of Hg(II) was also very weak, with the slope of the calibration curve of 1.47. This could be attributed to the fact that in the presence of other competing metal during simultaneous detection of heavy metals, the influence of the deposition current is distributed between all the competing ions in the electrochemical system and results in significantly less ion deposition, and thus reduced current response of the target ion is noted. The SWASV signals and the calibration curves of the HMs ions on Cu@AgNRs/FTO device (Figures 10b and 10d) demonstrate two linear ranges between the concentrations. The linear regression equation, the corresponding linear range, linear correlation coefficient and other performance parameters are summarized in Table 2. LODs with the signal-to-noise ratio of 3 (s/n = 3) were found to be 0.005 µM for Zn(II), 0.003 µM for Cd(II), 0.002 µM for Pb(II) and 0.02 µM for Hg(II), respectively. The Cu@AgNRs/FTO showed distinct peaks with a separation of 0.40, 0.25, and 0.51 V between Zn(II)-Cd(II), Cd(II)-Pb(II), and Pb(II)-Hg(II), respectively. These results indicate that the developed Cu@AgNRs/FTO-based electrochemical platform is capable of simultaneous detection of multiple HMs ions with high selectivity and sensitivity.

A noticeable variation in the sensitivity of HMs sensing in the individual and simultaneous analysis was observed. In the case of CuNRs/FTO-based device, there was a reduction of 7.0, 3.0, and 2.0 times in the LoD values for Zn(II), Pb(II), and Hg(II) during simultaneous HMs detection as compared to sensing of individual HMs. However, for Cd(II), there was no change in the LoD values, but a noticeable reduction

in the sensitivity from 130.75 to 104.3 $\mu A \cdot \mu M^{-1} \cdot cm^{-2}$ was observed. An overall decrease in the sensitivity was also observed in the case of other analyzed HMs. Similarly, in the case of the Cu@AgNRs/FTO based device, it can be seen that there is a decrease in LoD during the simultaneous detection of HMs by about 1.5, 2.0, and 5 times for Cd(II), Pb(II), and Hg(II), respectively. However, the sensitivity attained by Cu@AgNRs/FTO devices was much higher as compared to CuNRs/FTO devices. In the case of Zn(II), an increase in the LoD was observed for simultaneous detection of HMs as compared to individual HMs ions detection using Cu@AgNRs/FTO. This could be due to the presence of Hg film on the working electrode surface during the deposition period [38]. Though a decrease in the performance was observed during the simultaneous detection of HMs (with respect to individual sensing) at the Cu@AgNRs/FTO, the peaks were well- shaped with high resolution that could be instrumental for simultaneous determination of HMs with great accuracy.

The complex interaction between the two electron rich atoms in Cu@AgNRs could modify the surface electrical properties of these nanoparticles resulting in an enhanced electrical signal for the analytes. The lattice strain generated at the Ag-Cu interface due to the deformities is also known to enhance the electrocatalytic activities of bimetallic nanoparticles.[71] The resulting surface trapping and charge densification arising due to change in the interatomic bond lengths and change in the energy levels of the bonding electrons also could be a reason for the enhanced peak current in Cu@AgNRs/FTO based electrochemical platform.[21,72]

A comparison table providing various electrochemical sensing platforms with the proposed electrochemical systems is provided in Table S1 of the Supplementary Information. The FTO/ITO based electrochemical platforms for HMs sensing is very

sparsely reported in literatures. These reports are to sense only single heavy metal ions like Pb(II) [73] or Hg(II) [74]. Moreover, the proposed electrochemical platform is a miniaturized version of the conventional three electrode system. The earlier studies in the table used FTO as the working electrode only along with a traditional Pt wire (counter electrode) and Ag/AgCl reference electrode for the sensing experiments. A comparable sensing performance could be obtained using the proposed Cu@AgNRs and CuNRs/FTO based electrochemical system to the conventional glassy carbon electrode based electrochemical three electrode systems.

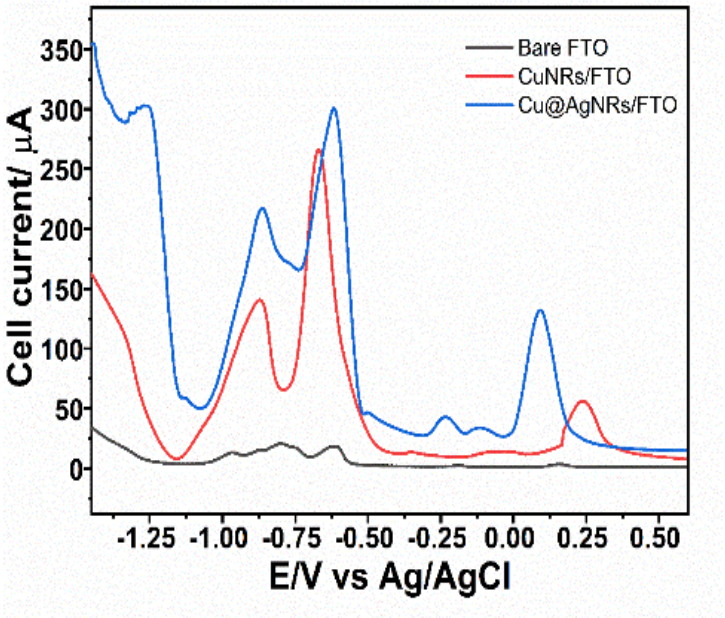

Figure 9: Simultaneous electrochemical sensing of Zn(II), Cd(II), Pb(II) and Hg(II) with various modified FTO based devices. Reaction conditions: HMs of 10 µM in acetate buffer at pH 5.0. Frequency was set at 15 Hz, amplitude 0.02 V, deposition 90 s, and conditioning time 30 s.

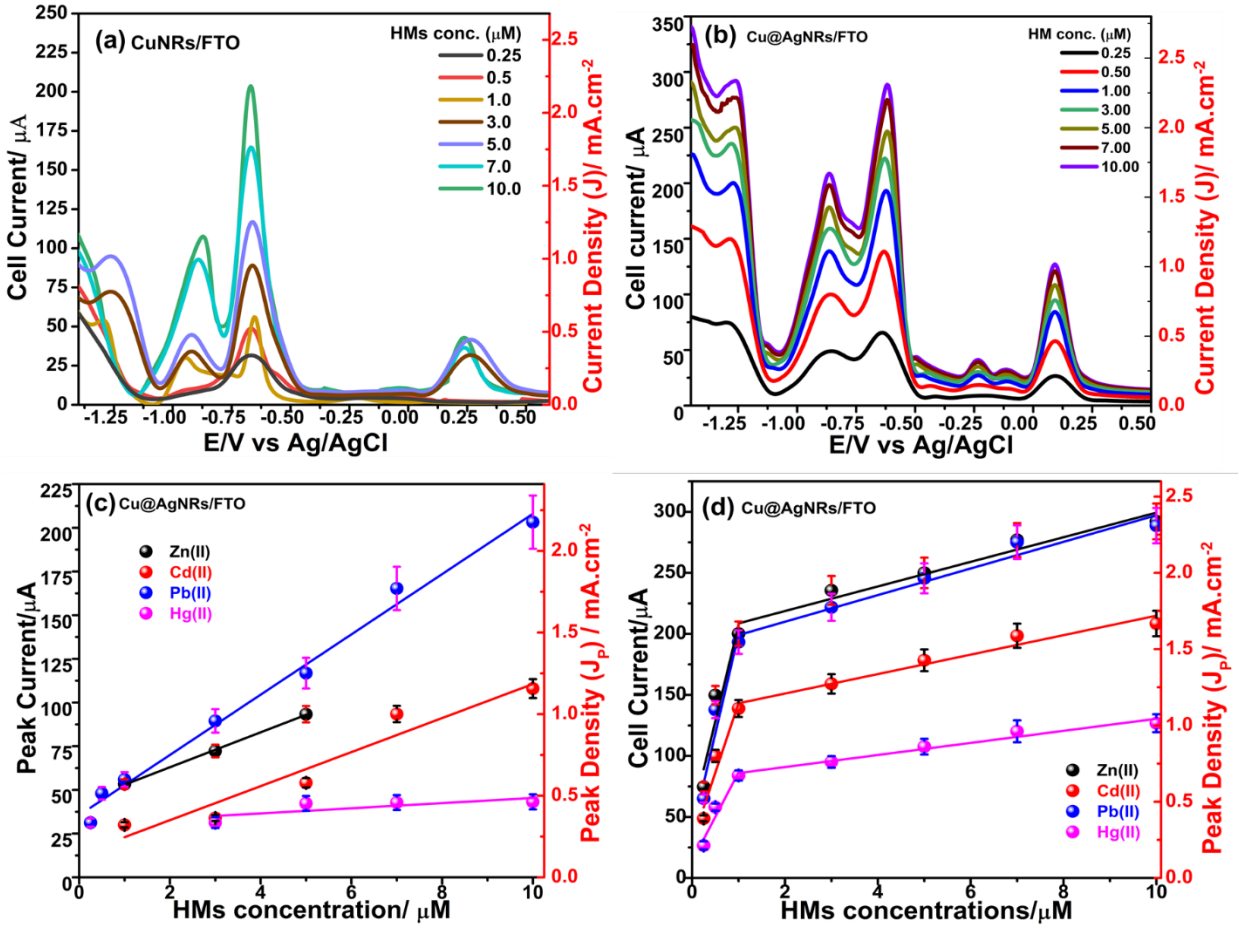

Figure 10: Square-wave voltammograms for simultaneous electrochemical sensing of Zn(II), Cd(II), Pb(II) and Hg(II) using (a) CuNRs/FTO and (b) Cu@AgNRs/FTO based devices, (c) Calibration curve with CuNRs/FTO, and (d) Calibration curves with Cu@AgNRs/FTO. Reaction conditions: HMs of 0.25-10 μM in acetate buffer at pH 5.0. Frequency was set at 15 Hz, amplitude 0.02 V, deposition time 90 s, and conditioning time 30 s.

Table 2: Fabricated sensor performance parameters for simultaneous HMs detection.

		CuNRs/FTO			
	Sensor parameters	**Zn(II)**	**Cd(II)**	**Pb(II)**	**Hg(II)**
	Permissible limits (USEPA, 2018) (μM)	76.5	0.044	0.072	0.015
CuNRs/FTO	Linear ranges (μM)	1.0-5.0	1.0-10.0	0.25 - 10	3.0-10.0
	Linear equation	I_{Pa}(μA) = 9.99[Zn(II)] μM + 43.00	I_{Pa}(μA) = 9.7[Cd(II)] μM + 13.23	I_{Pa}(μA) = 17.2[Pb(II)] μM + 35.53	I_{Pa}(μA) = 1.5[Hg(II)] μM + 30.64
	LoD (μM)	0.037	0.038	0.021	0.25
	LoQ (μM)	0.123	0.127	0.071	0.845
	Effective surface area (cm^2)	0.093			
	Sensitivity ($\mu A \cdot \mu M^{-1} \cdot cm^{-2}$)	107.4	104.6	185.4	15.9
Cu@AgNRs/FTO	Linear ranges (μM)	0.1-1 and 1-10			
	Linear equation	I_{Pa}(μA) = 29.4[Zn(II)] μM + 167.77	I_{Pa}(μA) = 131.0[Cd(II)] μM + 165.5	I_{Pa}(μA) = 150.2[Pb(II)] μM + 111.8	I_{Pa}(μA) = 52.6[Hg(II)] μM + 83.27
	LoD (μM)	0.005	0.003	0.002	0.025
	LoQ (μM)	0.017	0.01	0.006	0.08
	Effective surface area (cm^2)	0.125			
	Sensitivity ($\mu A \cdot \mu M^{-1} \cdot cm^{-2}$)	1261.8	912	1297.9	583.6

3.2.6 Reproducibility and repeatability analysis

The reproducibility of the CuNRs/FTO and Cu@AgNRs/FTO sensors was studied by intra-assay (n=3). Relative standard deviations (RSD) with Cu@AgNRs/FTO are estimated to be 2.2, 3.9, 0.98 and 4.6% for Zn(II), Cd(II), Pb(II) and Hg(II), respectively. These are far less than CuNRs/FTO sensors with RSD of 6.24, 3.59, 3.21, and 7.5%, respectively, for Zn(II), Cd(II), Pb(II) and Hg(II). These findings demonstrate that Cu@AgNRs/FTO based devices

could minimize the detection signal differences arising from the background conditions, and it could also increase the reproducibility of the electrochemical system by minimizing the formation of oxide layers which is very important for the sensing of HMs ions for field applications. The repeatability of the prepared devices was determined by running seven SWASV cycles using the same electrode. The SWASV signal is depicted in Figure. S5 of the Supplementary Information. The peak signal responses are shown in Figure 11. It can be observed that there is no significant variation in the peak currents up to 4 cycles after which there was a decrease in the peak current signal by about 35 and 19%, respectively for CuNRs/FTO and Cu@AgNRs after 7th cycle. This can be attributed to the delamination of the coatings from the base FTO during the stripping and deposition when the counter electrode (bare FTO) acted as an anode. This is a marked improvement in the reusability of the sensor compared to single use disposable screen-printed electrodes.

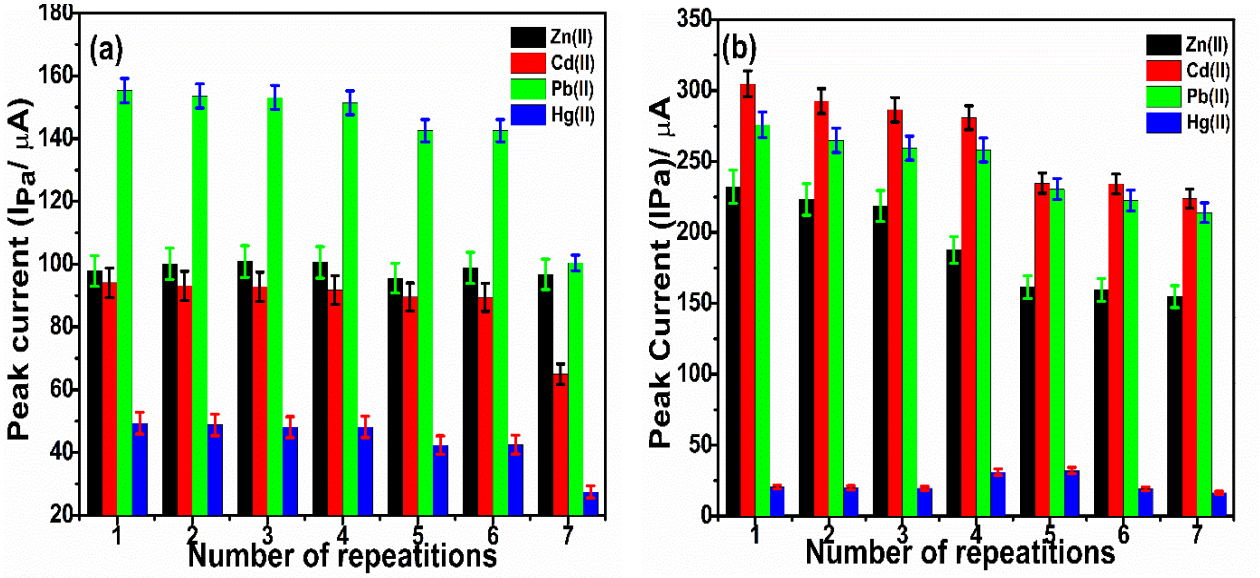

Figure 11: Repeatability (peak current) of HMs ions sensing using (a) CuNRs/FTO, and (b) Cu@AgNRs/FTO. Experimental conditions: HMs of 10 μM, acetate buffer (pH 5.0), square wave frequency 15 Hz, amplitude 0.02 V, deposition time 90 s, deposition potential -0.4 V, and conditioning time 30 s.

3.2.7 Environmental sample analysis

The developed Cu@AgNRs/FTO device was used for the detection of HMs present, if any, in real tap water and river water samples. The SWASV analysis for the quantification of the HMs was conducted as per the optimized parameters. In the environmental water samples, as can be seen in Figure 12, Zn(II), Cd(II), Pb(II) and Cu(II) stripping peaks cannot be found. It indicates that the concentration of HMs was below the LODs of the device, or that the target HMs ions were not present in these samples. Therefore, the water samples were further spiked by the target HMs, and distinct and well-separated SWASV peaks were found for Zn(II), Cd(II), Pb(II), and Hg(II). The collected water samples were analyzed for their anions content and the results are depicted in Figure S6(a) (river water) and Figure S6(b) (tap water) of the Supplementary Information. A very high concentration of PO_4^- (365.65 mg·L^{-1}) was present in the river water sample. Cl^- concentration was quite high (13.40 mg·L^{-1}) in the tap water samples. The presence of F^-, and SO_4^- was also evident from the analysis. The tap water and river water-based recovery experiment was performed using a standard supplement approach, and the results are presented in Table 3. The presence of interfering anions in the water sample did not show any significant adverse effects on the HMs quantification. In river water, the recovery value was obtained against a known spiked amount of HMs that were subjected for the simultaneous detection of the HMs, and the obtained values are 91.0 -92.2, 93.9-104.9, 94.2-109.8, and 86.7-98.76%, respectively with RSD values of 3.9, 2.4, 2.1 and 5.2%, respectively, for Zn(II), Cd(II), Pb(II) and Hg(II). Similarly, in tap water samples the recovery varied from 96.3-97.3, 98.7-103.3, 99.2-102.8, and 91.7-96.6%, respectively for Zn(II), Cd(II), Pb(II) and Hg(II). The RSD obtained for three replicates were 4.2, 2.2, 1.8, and 4.3%, respectively. These results clearly demonstrate that the proposed electrochemical sensors have

high accuracy and reliability for analysis of Zn(II), Cd(II), Pb(II), and Hg(II) in real environmental water samples.

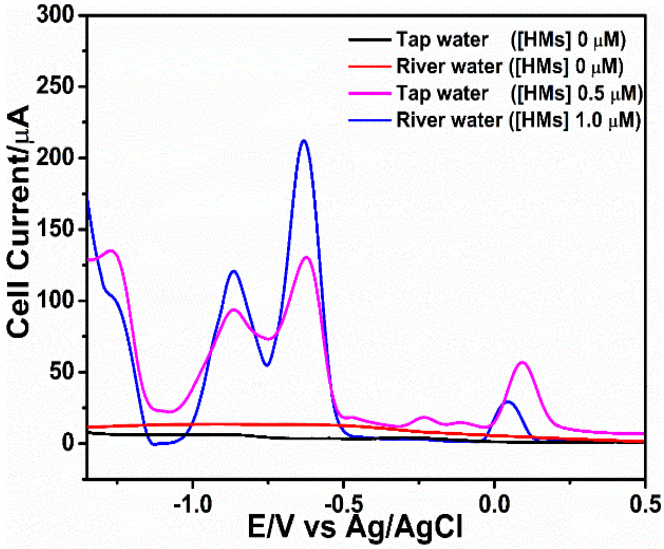

Figure 12: Square wave voltammetry signal for HMs in environmental water samples. Experimental conditions: Frequency was set at 15 Hz, amplitude 0.02 V, deposition time 90 s, and conditioning time 30 s at pH 5.

Table 2: Performance of Cu@AgNRs/FTO device for HMs detection from environmental water samples.

Sample	HMs (μM)	Zn(II)	Cd(II)	Pb(II)	Hg(II)
River water	0	ND	ND	ND	ND
River water	0.5	91.0	93.9	94.2	98.7
Tap water	1	92.2	104.9	109.8	86.7
	0	ND	ND	ND	ND
Tap water	0.5	97.3	98.8	99.2	96.6
	1	96.3	103.3	102.8	91.7

4. Conclusions

This study introduces a novel and cost-effective method for producing a miniaturized three-electrode system based on FTO. The FTO sheet was utilized to create a structured 3-electrode system using laser engraving techniques. A pseudo-reference electrode was incorporated into the system by applying a layer of Ag/AgCl ink. The fabricated device

enables the concurrent detection of heavy metals Zn(II), Cd(II), Pb(II), and Hg(II), and it exhibits reusability for up to four cycles. The devices exhibited exceptional analytical capabilities with regards to a significantly broad operational range encompassing two linear intervals: one ranging from 0.1 μM to 1 μM, and the other covering from 1 μM to 10 μM of heavy metal concentration. The sensors exhibited remarkable sensitivity, achieving low detection limits of 1 nM for Cd(II), 2 nM for Pb(II), 5 nM for Zn(II), and 6 nM for Hg(II) in individual detection, and 2 nM for Cd(II), 2 nM for Pb(II), 3 nM for Zn(II), and 4 nM for Hg(II) in simultaneous detection. The experimental results demonstrated strong repeatability and excellent recovery rates exceeding 90% during the assessment of heavy metal ions detection in environmental water samples. The sensors exhibited distinct peak-to-peak separation for different pairs of heavy metal ions. This demonstrates the efficacy of the manufactured device in accurately detecting heavy metal ions across a diverse range of environmental samples, while minimizing any notable interferences. Though a slight decrease in the sensitivity was observed during simultaneous heavy metal ion detection, the detection limits were well below the permissible limits (EPA guidelines) except for mercury. This shows the capability of the fabricated devices for successful determination of heavy metal ions in a wide variety of environmental water samples without any significant interferences.

Author Contributions

Smruti Ranjan Dash designed, carried out, and analysed most of the practical work and drafted the manuscript. Aruna Ivaturi directly supervised most of the work. Aruna Ivaturi, Animes Kumar Golder and Subhendu Sekhar Bag provided inputs to the manuscript, results interpretation, and manuscript correction.

Conflicts of interest

There are no conflicts to declare.

Acknowledgements

We gratefully acknowledge the Commonwealth Scholarship Commission, UK for providing the research funding for the project and sponsoring SRD (Ref: INCN-2019-126) under the Split-site Scholarship program-2019. We are grateful to Department of Pure and Applied Chemistry, University of Strathclyde, Glasgow and the Central Instruments Facility of Indian Institute of Technology Guwahati, for providing the necessary research facilities. AG and AI would like to acknowledge UK-India Education and Research Initiative (UKIERI) for the funding (DST-UKIERI 2017 18 - 009 (IND/CONT/G/17-18/39). AI acknowledges UK Research and Innovation (UKRI), Engineering and Physical Sciences Research Council (EPSRC) for the Fellowship grant (EP/P011500/1).

References

[1] R.A. Wuana, F.E. Okieimen, Heavy Metals in Contaminated Soils: A Review of Sources, Chemistry, Risks and Best Available Strategies for Remediation, ISRN Ecol. 2011 (2011) 1–20. https://doi.org/10.5402/2011/402647.

[2] A. Alengebawy, S.T. Abdelkhalek, S.R. Qureshi, M.Q. Wang, Heavy metals and pesticides toxicity in agricultural soil and plants: Ecological risks and human health implications, Toxics. 9 (2021) 1–34. https://doi.org/10.3390/toxics9030042.

[3] B.K. Bansod, T. Kumar, R. Thakur, S. Rana, I. Singh, A review on various electrochemical techniques for heavy metal ions detection with different sensing platforms, Biosens. Bioelectron. 94 (2017) 443–455. https://doi.org/10.1016/j.bios.2017.03.031.

[4] M. Moghtaderi, M.A. Ashraf, T. Moghtaderi, S.H. Teshnizi, S.H. Nabavizadeh, Heavy metal concentration in classroom dust samples and its relationship with childhood asthma: A study from islamic Republic of Iran, East. Mediterr. Heal. J. 26 (2020) 594–601. https://doi.org/10.26719/emhj.19.072.

[5] F. Gorini, F. Muratori, M.A. Morales, The Role of Heavy Metal Pollution in Neurobehavioral Disorders: a Focus on Autism, Rev. J. Autism Dev. Disord. 1 (2014) 354–372. https://doi.org/10.1007/s40489-014-0028-3.

[6] F.L. Migliorini, R.C. Sanfelice, A. Pavinatto, J. Steffens, C. Steffens, D.S. Correa, Voltammetric cadmium(II) sensor based on a fluorine doped tin oxide electrode modified with polyamide 6/chitosan electrospun nanofibers and gold nanoparticles, Microchim. Acta. 184 (2017) 1077–1084. https://doi.org/10.1007/s00604-017-2082-x.
[7] S. Singh, A. Numan, Y. Zhan, V. Singh, T. Van Hung, N.D. Nam, A novel highly efficient and ultrasensitive electrochemical detection of toxic mercury (II) ions in canned tuna fish and tap water based on a copper metal-organic framework, J. Hazard. Mater. 399 (2020) 123042. https://doi.org/10.1016/j.jhazmat.2020.123042.
[8] X. Qu, H. Yang, Z. Yu, B. Jia, H. Qiao, Y. Zheng, K. Dai, Serum zinc levels and multiple health outcomes: Implications for zinc-based biomaterials, Bioact. Mater. 5 (2020) 410–422. https://doi.org/10.1016/j.bioactmat.2020.03.006.
[9] X. Lu, J. Zhao, X. Liang, L. Zhang, Y. Liu, X. Yin, X. Li, B. Gu, The Application and Potential Artifacts of Zeeman Cold Vapor Atomic Absorption Spectrometry in Mercury Stable Isotope Analysis, Environ. Sci. Technol. Lett. 6 (2019) 165–170. https://doi.org/10.1021/acs.estlett.9b00067.
[10] A.A. Ammann, Speciation of heavy metals in environmental water by ion chromatography coupled to ICP-MS, Fresenius. J. Anal. Chem. 372 (2002) 448–452. https://doi.org/10.1007/s00216-001-1115-8.
[11] H. Ebrahimi-Najafabadi, A. Pasdaran, R. Rezaei Bezenjani, E. Bozorgzadeh, Determination of toxic heavy metals in rice samples using ultrasound assisted emulsification microextraction combined with inductively coupled plasma optical emission spectroscopy, Food Chem. 289 (2019) 26–32. https://doi.org/10.1016/j.foodchem.2019.03.046.
[12] S. Patra, A.K. Golder, R.V.S. Uppaluri, Ultrasensitive Colorimetric Detection and Determination of Hg(II) Using Bioinspired AgNPs Synthesized from Mature Camellia Sinensis Leaves, Results Opt. 11 (2023) 100411. https://doi.org/10.1016/j.rio.2023.100411.
[13] X. Liu, Y. Yao, Y. Ying, J. Ping, Recent advances in nanomaterial-enabled screen-printed electrochemical sensors for heavy metal detection, TrAC - Trends Anal. Chem. 115 (2019) 187–202. https://doi.org/10.1016/j.trac.2019.03.021.
[14] J. Barton, M.B.G. García, D.H. Santos, P. Fanjul-Bolado, A. Ribotti, M. McCaul, D. Diamond, P. Magni, Screen-printed electrodes for environmental monitoring of heavy metal ions: a review, Microchim. Acta. 183 (2016) 503–517. https://doi.org/10.1007/s00604-015-1651-0.
[15] G. Aragay, J. Pons, A. Merkoi, Enhanced electrochemical detection of heavy metals at heated graphite nanoparticle-based screen-printed electrodes, J. Mater. Chem. 21 (2011) 4326–4331. https://doi.org/10.1039/c0jm03751f.
[16] G. Cabello, R.A. Davoglio, F.W. Hartl, J.F. Marco, E.C. Pereira, S.R. Biaggio, H. Varela, A. Cuesta, Microwave-Assisted Synthesis of Pt-Au Nanoparticles with Enhanced Electrocatalytic Activity for the Oxidation of Formic Acid, Electrochim. Acta. 224 (2017) 56–63. https://doi.org/10.1016/j.electacta.2016.12.022.
[17] A. Londono-Calderon, C.A. Campos-Roldan, R.G. González-Huerta, M.L. Hernandez-Pichardo, P. del Angel, M.J. Yacaman, Influence of the architecture of Au–Ag–Pt nanoparticles on the electrocatalytic activity for hydrogen evolution reaction, Int. J. Hydrogen Energy. 42 (2017) 30208–30215. https://doi.org/10.1016/j.ijhydene.2017.08.042.
[18] J. Kim, C. Renault, N. Nioradze, N. Arroyo-Currás, K.C. Leonard, A.J. Bard, Electrocatalytic Activity of Individual Pt Nanoparticles Studied by Nanoscale Scanning

Electrochemical Microscopy, J. Am. Chem. Soc. 138 (2016) 8560–8568. https://doi.org/10.1021/jacs.6b03980.
[19] P.P. Fang, S. Duan, X.D. Lin, J.R. Anema, J.F. Li, O. Buriez, Y. Ding, F.R. Fan, D.Y. Wu, B. Ren, Z.L. Wang, C. Amatore, Z.Q. Tian, Tailoring Au-core Pd-shell Pt-cluster nanoparticles for enhanced electrocatalytic activity, Chem. Sci. 2 (2011) 531–539. https://doi.org/10.1039/c0sc00489h.
[20] A. Xu, L. Chao, H. Xiao, Y. Sui, J. Liu, Q. Xie, S. Yao, Ultrasensitive electrochemical sensing of Hg2+ based on thymine-Hg2+-thymine interaction and signal amplification of alkaline phosphatase catalyzed silver deposition, Biosens. Bioelectron. 104 (2018) 95–101. https://doi.org/10.1016/j.bios.2018.01.005.
[21] S.R. Dash, S.S. Bag, A.K. Golder, Synthesis of highly structured spherical Ag@Pt core-shell NPs using bio-analytes for electrocatalytic Pb(II) sensing, Sensors Actuators, B Chem. 314 (2020) 128062. https://doi.org/10.1016/j.snb.2020.128062.
[22] P. Niu, C. Fernández-Sánchez, M. Gich, C. Ayora, A. Roig, Electroanalytical assessment of heavy metals in waters with bismuth nanoparticle-porous carbon paste electrodes, Electrochim. Acta. 165 (2015) 155–161. https://doi.org/10.1016/j.electacta.2015.03.001.
[23] J. Gong, T. Zhou, D. Song, L. Zhang, Monodispersed Au nanoparticles decorated graphene as an enhanced sensing platform for ultrasensitive stripping voltammetric detection of mercury(II), Sensors Actuators, B Chem. 150 (2010) 491–497. https://doi.org/10.1016/j.snb.2010.09.014.
[24] K. Torres-Rivero, L. Torralba-Cadena, A. Espriu-Gascon, I. Casas, J. Bastos-Arrieta, A. Florido, Strategies for surface modification with ag-shaped nanoparticles: Electrocatalytic enhancement of screen-printed electrodes for the detection of heavy metals, Sensors (Switzerland). 19 (2019) 1–14. https://doi.org/10.3390/s19194249.
[25] S. Prakash, V.K. Shahi, Improved sensitive detection of Pb2+ and Cd2+ in water samples at electrodeposited silver nanonuts on a glassy carbon electrode, Anal. Methods. 3 (2011) 2134–2139. https://doi.org/10.1039/c1ay05265a.
[26] Y. Yang, M. Kang, S. Fang, M. Wang, L. He, J. Zhao, H. Zhang, Z. Zhang, Electrochemical biosensor based on three-dimensional reduced graphene oxide and polyaniline nanocomposite for selective detection of mercury ions, Sensors Actuators, B Chem. 214 (2015) 63–69. https://doi.org/10.1016/j.snb.2015.02.127.
[27] N. Promphet, P. Rattanarat, R. Rangkupan, O. Chailapakul, N. Rodthongkum, An electrochemical sensor based on graphene/polyaniline/polystyrene nanoporous fibers modified electrode for simultaneous determination of lead and cadmium, Sensors Actuators, B Chem. 207 (2015) 526–534. https://doi.org/10.1016/j.snb.2014.10.126.
[28] M. Lo, A.K.D. Diaw, D. Gningue-Sall, J.J. Aaron, M.A. Oturan, M.M. Chehimi, Tracking metal ions with polypyrrole thin films adhesively bonded to diazonium-modified flexible ITO electrodes, Environ. Sci. Pollut. Res. 25 (2018) 20012–20022. https://doi.org/10.1007/s11356-018-2140-x.
[29] Y. Zuo, J. Xu, X. Zhu, X. Duan, L. Lu, Y. Gao, H. Xing, T. Yang, G. Ye, Y. Yu, Poly(3,4-ethylenedioxythiophene) nanorods/graphene oxide nanocomposite as a new electrode material for the selective electrochemical detection of mercury (II), Synth. Met. 220 (2016) 14–19. https://doi.org/10.1016/j.synthmet.2016.05.022.
[30] L. Oularbi, M. Turmine, F.E. Salih, M. El Rhazi, Ionic liquid/carbon nanofibers/bismuth particles novel hybrid nanocomposite for voltammetric sensing of heavy metals, J. Environ. Chem. Eng. 8 (2020) 103774. https://doi.org/10.1016/j.jece.2020.103774.
[31] H. Wang, G. Zhao, Z. Zhang, Y. Yi, Z. Wang, G. Liu, A portable electrochemical

workstation using disposable screen-printed carbon electrode decorated with multiwall carbon nanotube-ionic liquid and bismuth film for Cd(II) and Pb(II) determination, Int. J. Electrochem. Sci. 12 (2017) 4702–4713. https://doi.org/10.20964/2017.06.73.
[32] S. Kim, Y. Jeong, M.O. Park, Y. Jang, J.S. Bae, K.S. Hong, S. Kim, P. Song, J.H. Yoon, Development of boron doped diamond electrodes material for heavy metal ion sensor with high sensitivity and durability, J. Mater. Res. Technol. 23 (2023) 1375–1385. https://doi.org/10.1016/j.jmrt.2023.01.116.
[33] E. Bernalte, S. Arévalo, J. Pérez-Taborda, J. Wenk, P. Estrela, A. Avila, M. Di Lorenzo, Rapid and on-site simultaneous electrochemical detection of copper, lead and mercury in the Amazon river, Sensors Actuators, B Chem. 307 (2020) 127620. https://doi.org/10.1016/j.snb.2019.127620.
[34] A. Hyder, S. Sanam Memon, S. Memon, Sirajuddin, Z. ul A. Memon, D. Bux Rajpar, S. Gul Shaikh, J. Ahmed Buledi, A highly discerning p-tetranitrocalix[4]arene (p-TNC4) functionalized copper nanoparticles: A smart electrochemical sensor for the selective determination of Diphenhydramine drug, Microchem. J. 163 (2021) 105908. https://doi.org/10.1016/j.microc.2020.105908.
[35] J.R. Camargo, L.O. Orzari, D.A.G. Araújo, P.R. de Oliveira, C. Kalinke, D.P. Rocha, A. Luiz dos Santos, R.M. Takeuchi, R.A.A. Munoz, J.A. Bonacin, B.C. Janegitz, Development of conductive inks for electrochemical sensors and biosensors, Microchem. J. 164 (2021). https://doi.org/10.1016/j.microc.2021.105998.
[36] N. Wannasri, P. Uppachai, N. Butwong, S. Jantrasee, I.M. Isa, S. Loiha, S. Srijaranai, S. Mukdasai, A facile nonenzymatic electrochemical sensor based on copper oxide nanoparticles deposited on activated carbon for the highly sensitive detection of methyl parathion, J. Appl. Electrochem. 52 (2022) 595–606. https://doi.org/10.1007/s10800-021-01642-1.
[37] P. Sundaresan, C.C. Fu, S.H. Liu, R.S. Juang, Facile synthesis of chitosan-carbon nanofiber composite supported copper nanoparticles for electrochemical sensing of carbendazim, Colloids Surfaces A Physicochem. Eng. Asp. 625 (2021) 126934. https://doi.org/10.1016/j.colsurfa.2021.126934.
[38] D. Li, C. Wang, H. Zhang, Y. Sun, Q. Duan, J. Ji, W. Zhang, S. Sang, A highly effective copper nanoparticle coupled with RGO for electrochemical detection of heavy metal ions, Int. J. Electrochem. Sci. 12 (2017) 10933–10945. https://doi.org/10.20964/2017.11.19.
[39] Z. Kheibarian, E. Soleimani, H.R. Mardani, Green synthesis of Cu@Ag core–shell nanoparticles as efficient colorimetric sensing for Hg(II) ion, Appl. Phys. A Mater. Sci. Process. 128 (2022). https://doi.org/10.1007/s00339-022-05515-y.
[40] A. Sakthisabarimoorthi, M. Jose, S.A. Martin Britto Dhas, S. Jerome Das, Fabrication of Cu@Ag core–shell nanoparticles for nonlinear optical applications, J. Mater. Sci. Mater. Electron. 28 (2017) 4545–4552. https://doi.org/10.1007/s10854-016-6090-0.
[41] Y. Ying, R. Gao, Y. Hu, Y. Long, Electrochemical Confinement Effects for Innovating New Nanopore Sensing Mechanisms, Small Methods. 2 (2018) 1700390. https://doi.org/10.1002/smtd.201700390.
[42] S.M. Lu, Y.Y. Peng, Y.L. Ying, Y.T. Long, Electrochemical Sensing at a Confined Space, Anal. Chem. 92 (2020) 5621–5644. https://doi.org/10.1021/acs.analchem.0c00931.
[43] S.L. Ting, S.J. Ee, A. Ananthanarayanan, K.C. Leong, P. Chen, Graphene quantum dots functionalized gold nanoparticles for sensitive electrochemical detection of heavy metal ions, Electrochim. Acta. 172 (2015) 7–11.

https://doi.org/10.1016/j.electacta.2015.01.026.
[44] Y. Wei, C. Gao, F.L. Meng, H.H. Li, L. Wang, J.H. Liu, X.J. Huang, SnO 2/reduced graphene oxide nanocomposite for the simultaneous electrochemical detection of cadmium(II), lead(II), copper(II), and mercury(II): An interesting favorable mutual interference, J. Phys. Chem. C. 116 (2012) 1034–1041. https://doi.org/10.1021/jp209805c.
[45] Y. Zhang, Y. Wang, J. Jia, J. Wang, Nonenzymatic glucose sensor based on graphene oxide and electrospun NiO nanofibers, Sensors Actuators, B Chem. 171–172 (2012) 580–587. https://doi.org/10.1016/j.snb.2012.05.037.
[46] M. Fayazi, M. Ghanei-Motlagh, C. Karami, Application of magnetic nanoparticles modified with L-cysteine for pre-concentration and voltammetric detection of copper(II), Microchem. J. 181 (2022) 107652. https://doi.org/10.1016/j.microc.2022.107652.
[47] A. Capasso, S. Bellani, A.L. Palma, L. Najafi, A.E. Del Rio Castillo, N. Curreli, L. Cinà, V. Miseikis, C. Coletti, G. Calogero, V. Pellegrini, A. Di Carlo, F. Bonaccorso, CVD-graphene/graphene flakes dual-films as advanced DSSC counter electrodes, 2D Mater. 6 (2019) 035007. https://doi.org/10.1088/2053-1583/ab117e.
[48] V.V. Nguyen, T.H. Hoang Nguyen, C.M.T. Nguyen, H.L. Ngo, T.T. Nguyen, V.H. Le, T.H. Nguyen, A fast fabrication technique of FTO/AuNPs electrochemical electrodes for on-site arsenic (III) detection, Adv. Nat. Sci. Nanosci. Nanotechnol. 14 (2023) 045006. https://doi.org/10.1088/2043-6262/ad010a.
[49] S. Yokoyama, K. Motomiya, B. Jeyadevan, K. Tohji, Environmentally friendly synthesis and formation mechanism of copper nanowires with controlled aspect ratios from aqueous solution with ascorbic acid, J. Colloid Interface Sci. 531 (2018) 109–118. https://doi.org/10.1016/j.jcis.2018.07.036.
[50] I.E. Stewart, S. Ye, Z. Chen, P.F. Flowers, B.J. Wiley, Synthesis of Cu-Ag, Cu-Au, and Cu-Pt Core-Shell Nanowires and Their Use in Transparent Conducting Films, Chem. Mater. 27 (2015) 7788–7794. https://doi.org/10.1021/acs.chemmater.5b03709.
[51] Y.Q. Liu, M. Zhang, F.X. Wang, G.B. Pan, Facile microwave-assisted synthesis of uniform single-crystal copper nanowires with excellent electrical conductivity, RSC Adv. 2 (2012) 11235–11237. https://doi.org/10.1039/c2ra21578k.
[52] K. Anandalakshmi, J. Venugobal, V. Ramasamy, Characterization of silver nanoparticles by green synthesis method using Pedalium murex leaf extract and their antibacterial activity, Appl. Nanosci. 6 (2016) 399–408. https://doi.org/10.1007/s13204-015-0449-z.
[53] S. Arya, Prerna, A. Singh, R. Kour, Comparative study of CuO, CuO@Ag and CuO@Ag:La nanoparticles for their photosensing properties, Mater. Res. Express. 6 (2019). https://doi.org/10.1088/2053-1591/ab49ab.
[54] S. Gupta, P. Pandotra, A.P. Gupta, J.K. Dhar, G. Sharma, G. Ram, M.K. Husain, Y.S. Bedi, Volatile (As and Hg) and non-volatile (Pb and Cd) toxic heavy metals analysis in rhizome of Zingiber officinale collected from different locations of North Western Himalayas by Atomic Absorption Spectroscopy, Food Chem. Toxicol. 48 (2010) 2966–2971. https://doi.org/10.1016/j.fct.2010.07.034.
[55] I. Lisiecki, A. Filankembo, H. Sack-Kongehl, K. Weiss, M. Pileni, Structural investigations of copper nanorods by high-resolution TEM, Phys. Rev. B - Condens. Matter Mater. Phys. 61 (2000) 4968–4974. https://doi.org/10.1103/PhysRevB.61.4968.
[56] M. Luo, A. Ruditskiy, H.C. Peng, J. Tao, L. Figueroa-Cosme, Z. He, Y. Xia, Penta-Twinned Copper Nanorods: Facile Synthesis via Seed-Mediated Growth and Their

Tunable Plasmonic Properties, Adv. Funct. Mater. 26 (2016) 1209–1216. https://doi.org/10.1002/adfm.201504217.
[57] N. Ahmad, S. Sharma, K. Alam, V.N. Singh, S.F. Shamsi, B.R. Mehta, A. Fatma, Colloids and Surfaces B : Biointerfaces Rapid synthesis of silver nanoparticles using dried medicinal plant of basil, Colloids Surfaces B Biointerfaces. 81 (2010) 81–86. https://doi.org/10.1016/j.colsurfb.2010.06.029.
[58] T.C. Prathna, N. Chandrasekaran, A. Mukherjee, Colloids and Surfaces A : Physicochemical and Engineering Aspects Studies on aggregation behaviour of silver nanoparticles in aqueous matrices : Effect of surface functionalization and matrix composition, Colloids Surfaces A Physicochem. Eng. Asp. 390 (2011) 216–224. https://doi.org/10.1016/j.colsurfa.2011.09.047.
[59] M.A. Macdonald, H.A. Andreas, Method for equivalent circuit determination for electrochemical impedance spectroscopy data of protein adsorption on solid surfaces, Electrochim. Acta. 129 (2014) 290–299. https://doi.org/10.1016/j.electacta.2014.02.046.
[60] M. Shi, Z. Chen, J. Sun, Determination of chloride diffusivity in concrete by AC impedance spectroscopy, Cem. Concr. Res. 29 (1999) 1111–1115. https://ac.els-cdn.com/S0008884699000794/1-s2.0-S0008884699000794-main.pdf?_tid=60a80a13-b81a-478e-852e-59eb79b8d683&acdnat=1540492035_479b64f3451b4e184909ff10669d8318.
[61] A. Agee, T.M. Gill, G. Pace, R. Segalman, A. Furst, Electrochemical Characterization of Biomolecular Electron Transfer at Conductive Polymer Interfaces, J. Electrochem. Soc. 170 (2023) 016509. https://doi.org/10.1149/1945-7111/acb239.
[62] S.R. Dash, S.S. Bag, A.K. Golder, Bio-inspired PtNPs/Graphene nanocomposite based electrocatalytic sensing of metabolites of dipyrone, Anal. Chim. Acta. 1167 (2021) 338562. https://doi.org/10.1016/j.aca.2021.338562.
[63] M. Baghayeri, H. Alinezhad, M. Fayazi, M. Tarahomi, R. Ghanei-Motlagh, B. Maleki, A novel electrochemical sensor based on a glassy carbon electrode modified with dendrimer functionalized magnetic graphene oxide for simultaneous determination of trace Pb(II)and Cd(II), Electrochim. Acta. 312 (2019) 80–88. https://doi.org/10.1016/j.electacta.2019.04.180.
[64] F. De Lima, G. Maia, Oxidized/reduced graphene nanoribbons facilitate charge transfer to the Fe(CN)63-/Fe(CN)64- redox couple and towards oxygen reduction, Nanoscale. 7 (2015) 6193–6207. https://doi.org/10.1039/c5nr01123j.
[65] S.R. Dash, S.S. Bag, A.K. Golder, Carbon Dots Derived from Waste Psidium Guajava Leaves for Electrocatalytic Sensing of Chlorpyrifos, Electroanalysis. (2022). https://doi.org/10.1002/elan.202100344.
[66] G.M.S. Alves, J.M.C.S. Magalhães, H.M.V.M. Soares, Voltammetric Quantification of Zn and Cu, Together with Hg and Pb, Based on a Gold Microwire Electrode, in a Wider Spectrum of Surface Waters, Electroanalysis. 25 (2013) 493–502. https://doi.org/10.1002/elan.201200518.
[67] G. Zhao, H. Wang, G. Liu, Direct quantification of Cd2+ in the presence of Cu2+ by a combination of anodic stripping voltammetry using a Bi-film-modified glassy carbon electrode and an artificial neural network, Sensors (Switzerland). 17 (2017). https://doi.org/10.3390/s17071558.
[68] K. Xu, C. Pérez-Ràfols, A. Marchoud, M. Cuartero, G.A. Crespo, Anodic stripping voltammetry with the hanging mercury drop electrode for trace metal detection in soil samples, Chemosensors. 9 (2021). https://doi.org/10.3390/chemosensors9050107.

[69] Z. Wang, K. Yliniemi, E.L. Rautama, P.M. Hannula, B.P. Wilson, M. Lundström, Electrochemical Growth of Ag/Zn Alloys from Zinc Process Solutions and Their Dealloying Behavior, ACS Sustain. Chem. Eng. 10 (2022) 3716–3725. https://doi.org/10.1021/acssuschemeng.2c00284.
[70] C.E. Rahm, P. Gupta, V.K. Gupta, A. Huseinov, B. Griesmer, N.T. Alvarez, Impact of physical and chemical parameters on square wave anodic stripping voltammetry for trace Pb2+ detection in water, Analyst. 147 (2022) 3542–3557. https://doi.org/10.1039/d2an00724j.
[71] D. Chen, D. Wang, Q. Ge, G. Ping, M. Fan, L. Qin, L. Bai, C. Lv, K. Shu, Graphene-wrapped ZnO nanospheres as a photocatalyst for high performance photocatalysis, Thin Solid Films. 574 (2015) 1–9. https://doi.org/10.1016/j.tsf.2014.11.051.
[72] G. Ouyang, W.G. Zhu, C.Q. Sun, Z.M. Zhu, S.Z. Liao, Atomistic origin of lattice strain on stiffness of nanoparticles, Phys. Chem. Chem. Phys. 12 (2010) 1543–1549. https://doi.org/10.1039/b919982a.
[73] K. Saeteaw, G. Tumcharern, P. Piyakulawat, U. Asawapirom, S. Porntheeraphat, P. Duangkaew, R. Maolanon, R. Piyananjaratsri, J. Nukeaw, S. Pratontep, Heavy metal detection by electrochemical electronic tongue with poly(thiophene)-metal oxide nanoparticle composite electrodes, in: 2011 IEEE Nanotechnol. Mater. Devices Conf., IEEE, 2011: pp. 446–449. https://doi.org/10.1109/NMDC.2011.6155403.
[74] C.C. Fu, C. Te Hsieh, R.S. Juang, S. Gu, Y. Ashraf Gandomi, R.E. Kelly, K.D. Kihm, Electrochemical sensing of mercury ions in electrolyte solutions by nitrogen-doped graphene quantum dot electrodes at ultralow concentrations, J. Mol. Liq. 302 (2020) 112593. https://doi.org/10.1016/j.molliq.2020.112593.